Journal of Magnetic Resonance 383 (2026) 108010

Contents lists available at ScienceDirect

Journal of Magnetic Resonance

journal homepage: www.elsevier.com/locate/jmr

Simple setup for *in situ* electrochemical electron paramagnetic resonance spectroscopy to study organic energy-storage materials

Anatoliy A. Vereshchagin [a], Maryam Seif-Eddine [b], Kaltum Abdiaziz [c], Maxie M. Roessler [b], Oleg V. Levin [d], Jan Behrends [a,1,*]

[a] Berlin Joint EPR Lab, Fachbereich Physik, Freie Universität Berlin, Arnimallee 14, 14195 Berlin, Germany
[b] Department of Chemistry and Centre for Pulse EPR Spectroscopy, Molecular Sciences Research Hub, Imperial College London, London, UK
[c] Max Planck Institute for Chemical Energy Conversion, Mülheim an der Ruhr, Germany
[d] Saint Petersburg State University, 7/9 Universitetskaya nab., 199034 St. Petersburg, Russia

ARTICLE INFO

Keywords:
Electron paramagnetic resonance spectroscopy
Spectroelectrochemistry
Cyclic voltammetry
In situ technique
Organic battery materials
In-tube electrochemical cells
Cheap setup

ABSTRACT

The design and application of a cost-effective, customisable electrochemical cell suitable for *in situ* X-band (9–10 GHz) Electron Paramagnetic Resonance (EPR) experiments is demonstrated. The cell is optimized for investigating electrochemical parameters of redox-active polymer films at room temperature using polar organic electrolytes. The polymer film to be studied is directly deposited onto the surface of a platinum wire acting as the working electrode. The three-electrode cylindrical cell design with mutual arrangement of the electrodes, inspired by the "ultramicroelectrode concept", provides enhanced electrochemical response by minimizing ohmic drop while maintaining flexibility for a wide range of experimental setups. The cell performance is demonstrated using a redox conducting polymeric cathode material for organic radical batteries, namely poly[N, N″-bis(3-(4-oxy(2,2,6,6-tetramethylpiperidin-1-oxyl)butoxy)salicylidene)ethylenediiminato nickel(II)], as a test material. Continuous-wave EPR experiments using a portable benchtop spectrometer at a fixed magnetic field allow detecting the material's state of charge, initialisation of oxidation and reduction processes, as well as estimating electrochemical properties. The cell design presented here enables potentiostatic, galvanostatic, and potentiodynamic measurement modes, while offering the possibility of customisation through 3D printing and the use of various electrode materials.

1. Introduction

Unpaired electrons play a crucial role in many fundamental processes in materials and electrochemical devices for energy storage and energy conversion. In consequence, the spins associated with localised radicals as well as mobile charge carriers can be used as probes that provide useful insights into operational principles and loss mechanisms by electron paramagnetic resonance (EPR) spectroscopy. Whenever the redox state of active species changes and a conversion between paramagnetic and diamagnetic states occurs during device operation, *in situ* EPR techniques can be applied to identify functionally active paramagnetic sites and explore their electronic and geometric structure. Such studies have revealed important information about redox active species in various electrochemical systems such as protein films [1,2], intermediates and organic molecules [3,4], catalysts [5–9], lithium-ion batteries [10–12], redox-flow batteries [13] and organic radical batteries (ORBs) [14].

Conducting *in situ* EPR experiments is challenging due to significant dielectric losses at microwave frequencies when using polar solvents. Various *in situ* cell designs aim at minimizing the active electrolyte volume [15–17]. One popular design is based on a flat cell, in which the sample is placed in a non-standard rectangular tube, allowing the use of a smaller volume of electrolyte [14]. The main problems associated with these designs are a significant ohmic drop between the electrodes [18], difficult assembly and non-renewable electrode surface, as well as reduced EPR sensitivity due to the interaction of the microwave with the metal electrodes [16]. Alternatively, standard three-electrode cylindrical cells [19] or the so-called "ultramicroelectrode concept" [20]

* Corresponding author.
E-mail addresses: j.behrends@fu-berlin.de, jan.behrends@helmholtz-berlin.de (J. Behrends).
[1] Present address: Department Spins in Energy Conversion and Quantum Information Science (ASPIN), Helmholtz-Zentrum Berlin für Materialien und Energie, Hahn-Meitner-Platz 1, 14109 Berlin, Germany.

https://doi.org/10.1016/j.jmr.2025.108010
Received 16 May 2025; Received in revised form 5 December 2025; Accepted 15 December 2025
Available online 18 December 2025
1090-7807/© 2025 The Authors. Published by Elsevier Inc. This is an open access article under the CC BY license (http://creativecommons.org/licenses/by/4.0/).

provide a better electrochemical response due to minimized ohmic drop, although the typically used small electrodes can make detecting low concentration of EPR-active particles challenging. However, this design provides experimental flexibility and can be tailored for specific samples and measurement configurations. For example, it is possible to convert the cell into a flow cell using two or three electrodes, to work with dissolved particles, or by increasing the electrode area to work with active materials directly deposited onto the electrode.

Since a modern trend in materials science for various applications is the development of complex, hybrid systems, composite materials, combined molecules, macromolecules, and metal-organic frameworks (MOFs) of various structures, we explored the possibilities of *in situ* Film-Electrochemical EPR (FE-EPR) methods for analysing complex materials in order to assess the contribution of the individual components. As a test object we selected nitroxyl-containing redox-conductive polymers (RCP), which are promising alternatives to inorganic-based energy storage materials and efficient in-film catalytic systems due to their high energy density and fast redox kinetics [21–23]. Charge transfer processes in RCPs involve two redox centres: polaron/bipolaron fragments and radical-bearing groups, making their joint oxidation/reduction mechanism difficult to analyse. It was shown that *ex-* and *in situ* EPR spectroscopy methods can provide valuable insights into the nature and energy of generated radical species, reaction mechanisms, and interactions between redox centres and their environment [15,24].

In this work we present an alternative cost-effective and accessible cylindrical type electrochemical cell design for *in situ* room-temperature EPR experiments in the X-band microwave frequency range (9 to 10 GHz) that is compatible with a benchtop EPR spectrometer. The redox-active film to be studied is directly deposited onto the surface of a platinum wire acting as the working electrode. The functionality of the cell is demonstrated by performing *in situ* EPR measurements during oxidizing and reducing a film of poly[N,N″-bis(3-(4-oxy(2,2,6,6-tetramethylpiperidin-1-oxyl)butoxy)salicylidene)ethylenediiminato nickel (II)] (pDiTBuS) – a promising active electrode materials for ORBs – using Et_4NBF_4 / CH_3CN as a polar organic electrolyte. In particular, we show that two different modes of operation are possible, namely (1) recording a full EPR spectrum and (2) monitoring the EPR signal intensity at a fixed magnetic field during a cyclic voltammetry experiment. The second approach allows us to detect changes in the number of EPR-active sites with sub-second time resolution.

2. Experimental details

2.1. Cell design

The components and the complete schematic of the cell designed for *in situ* continuous wave (cw) EPR measurements are shown in Fig. 1 (see also Fig. S1 for more details).

We developed the cell based on previously reported designs [9,16,17,20,25] taking into account the specifics of working with polar organic solvents and with active materials directly deposited onto the working electrode by electropolymerisation.

The top part of Fig. 1 shows the main components of the cell: shell, counter electrode (CE), working electrode (WE) and reference electrode (RE). At the bottom, the assembled cell used in this work is presented. Cell versions A and B show possible modifications.

The cell's shell consists of two parts. The upper part is made from a PVC tube with an outer diameter of 3.9 mm and a wall thickness of 0.5 mm. The flexible tube hosts the wires and can be easily connected to the lower part of the cell without the use of adhesives or additional EPR active components. The lower part of the cell is made of a sealed Eppendorf epT.I.P.S. 20 µL polypropylene pipette tip with a length of 20 mm. The tip was sealed by heating the bottom open part to 165 °C using a soldering tool. The resulting drop of liquid polypropylene filled the void at the bottom of the tip and then solidified, forming a rigid layer impermeable to electrolyte. The outer diameter of the upper and sealed lower part of the tip is 3.9 mm and 2.0 mm, respectively. Since the inner diameter of the PVC tube is 1 mm smaller than the outer diameter of the pipette tip, when putting the tube on the tip, a rigid connection is formed (the polymer tube envelops the tip) between the elements. Without mechanical load the connection is stable and allows to work with solvents without leaks. The pipette tip was chosen due to its inertness with respect to the chosen electrolytes, low cost and absence of EPR signals. Its conical shape makes it possible to reduce the amount of polar solvent in the active volume of the microwave resonator while maintaining a clear electrochemical response. The diameter of the part at the connection between the PVC tube and the tip was 5 mm and was limited by the 5.1 mm inner diameter of the Nitrogen Dewar used in the EPR

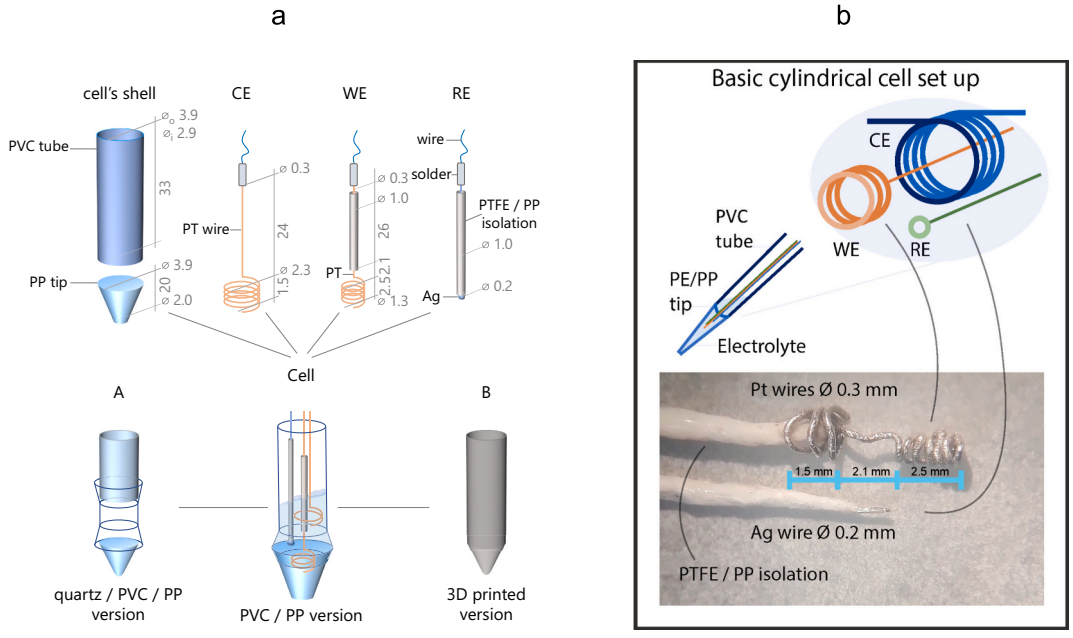


Fig. 1. Schematic representation of the electrochemical cell for room-temperature *in situ* EPR measurements (a) and photograph of the wire configuration (b). All dimensions are in millimeters, all schematic blocks are not drawn to scale.

spectrometer.

The CE is made of a platinum wire with a diameter of 0.3 mm with a spiral-shaped end. The diameter of the spiral was 2.3 mm and the length was 2.0 mm. The length of the straight part was 24 mm.

For the WE and RE an insulating layer was used to prevent short circuits as well as vertical diffusion of the electrolyte along the cell wires. The layer consists of PTFE Thread Seal Tape (100 μm thick) impregnated with molten polypropylene, which prevents the layer from being soaked with electrolyte. For that purpose the polypropylene tube was melted to 170 °C to a liquid state and applied in drops to the surface of the wire with insulated Teflon tape. The diameter of the electrodes at the insulation point was 1 mm. The WE made of a platinum wire (diameter of 0.3 mm) with a spiral-shaped end (diameter of 1.3 mm and length of 2.5 mm, 7 turns, surface area ~ 20.7 mm^2). The spiral electrode shape allows us to achieve a surface area about 9 times larger than that of an untwisted wire of the same active length (2.5 mm). It was created by winding the wire around a steel rod. The WE can be easily cleaned by calcining the wire on a burner, which allows one electrode to be used multiple times. When annealing, there is a chance of damaging the insulation between the counter and the working electrode. In this case, in the absence of a short circuit this is not a problem. Otherwise, the insulation has to be renewed. The distance between the insulating layer and the spiral was 2.1 mm. The insulating section had a length of 26 mm.

The RE is made of a silver wire with a diameter of 0.2 mm. The length of the insulated part was 29 mm, and the length of the non-insulated lower section was 1.1 mm.

Tin plated copper wire (Metrofunk Kabel Union LWPC20, 0.14 mm^2 cross-section area) was soldered to the upper part of electrodes.

For the assembly of the cell comprising all four elements, the working electrode is passed through the counter-electrode spiral. Further, the reference electrode is brought close to the area between the top of the working electrode spiral and the end of the counter electrode spiral in order to minimize the electrolyte resistance. The electrodes are additionally wrapped with Teflon tape in the upper part to improve mechanical stability. A small amount of electrolyte (60–80 μL) is placed in the shell, then the electrically connected electrodes are inserted. To compensate for possible evaporation of active electrolyte volume around the electrodes during long measurements, a 150 μL electrolyte reservoir above the active volume can be used. We kept the electrolyte level well above the three electrodes, up to ~1.7 cm from the bottom. In this work, the shell was also inserted from top into a long PVC tube, allowing the cell to be easily inserted and removed from the resonator. In this form, the cell can be inserted into the resonator and connected to the potentiostat. The long PVC tube can be replaced by a standard EPR quartz tube with an unsealed end, to which the shell is attached by simply pushing on the free section of a short PVC tube (Fig. 1, cell version A). We assume that the shell can also be made of any suitable material for 3D printing (Fig. 1, cell version B). The main criterion is the absence of an EPR signal and the inertness of the materials. For aqueous electrolytes, high Impact Polystyrene (HIPS), polylactic acid (PLA), polyethylene terephthalate (PET) and acrylonitrile butadiene styrene (ABS) are suitable, although some of these materials have low EPR activity. For acetonitrile solutions, which are used in this work, nylon or glass-fiber reinforced nylon are more suitable candidates.

2.2. Chemicals

The monomer complex [N,N″-bis(3-(4-oxy(2,2,6,6-tetramethylpiperidin-1-oxyl)butoxy)salicylidene)ethylenediiminato nickel(II)] - DiTBuS (Fig. 2) was synthesized by condensation of the previously obtained TEMPO-containing benzaldehyde [26] with ethylene diamine and subsequent complexation with nickel acetate in an ethanol medium. The monomer was purified by recrystallization from aqueous ethanol, after which it was dried under vacuum using a vacuum oil pump at room temperature.

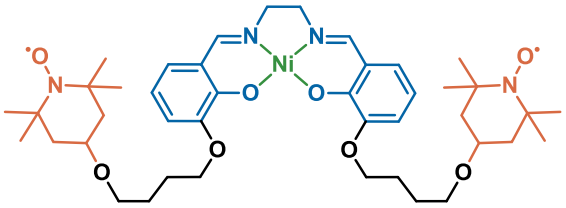


Fig. 2. Structure of the DiTBuS complex.

Commercial tetraethylammonium tetrafluoroborate (Et_4NBF_4, 99 %), CH_3CN (99.8 %, anhydrous), 3 Å molecular sieves were purchased from Sigma-Aldrich, silver nitrate (99.5 %) was purchased from Fluka. All purchased substances were used without further purification. 0.1 M and 1 M electrolyte solutions were stored under 3 Å molecular sieves.

2.3. Electrochemical measurements

Electrochemical experiments were carried out in 0.1 M or 1 M Et_4NBF_4 / CH_3CN electrolyte solutions using an Autolab PGSTAT204 potentiostat in standard three-electrode cells or the cell for *in situ* EPR.

A non-aqueous Ag| 1 mM $AgNO_3$, 0.1 M Et_4NBF_4 (CH_3CN) electrode (MF-2062, Bioanalytical systems) (0.3 V *vs.* Ag|AgCl ($NaCl_{sat}$), −0.133 V *vs.* Fc/Fc^+ [27] in CH_3CN) was used as a RE for in-beaker experiments (deposition and cleaning procedures). An Ag wire (+ 0.3 V *vs.* non-aqueous Ag| 1 mM $AgNO_3$, 0.1 M Et_4NBF_4 (CH_3CN) electrode) with a diameter of 0.2 mm was used as a RE in the EPR setup. Potentials are referenced to the electrode used (Ag| 1 mM $AgNO_3$, CH_3CN) or, if explicitly mentioned, to the Ag wire used for the *in situ* EPR measurements.

A coiled Pt wire with d = 1 mm was used as CE for the in-beaker experiments and with d = 0.3 mm for both CE and WE for the *in situ* EPR measurements.

The polymer film was deposited on the WE using 10 cycles of cyclic voltammetry (CV) electrochemical polymerisation with a potential scan rate of 50 mV s^{-1} from 1 mM solutions of the corresponding monomers in 0.1 M Et_4NBF_4 (CH_3CN) electrolyte in the potential range from −0.4 V to +0.9 V, thoroughly washed by acetonitrile using rinsing and CV in clean monomer-free solution and dried in air.

In situ FE-EPR / electrochemical performance tests were carried out using both cyclic voltammetry and galvanostatic charge-discharge (GCD) methods in a monomer-free 1 M Et_4NBF_4 (CH_3CN) electrolyte solution. The CV tests in the beaker were performed within the −0.4 V to 0.9 V potential range (or 0.1 + 1.1 V *vs.* Ag wire in the EPR setup) using scan rates between 5 mV s^{-1} and 50 mV s^{-1}.

The GCD tests were carried out in a three-electrode EPR setup cell using symmetric mode (*i.e.*, $I_{ch} = I_{disch}$) for charging and discharging at a current rate of 25C (0.025 mA cm^{-2} or 18 μA) in a − 0.4 V to 1.4 V potential range.

2.4. Continuous wave electron paramagnetic resonance

Room-temperature *ex situ* continuous wave electron paramagnetic resonance (cwEPR) spectra were recorded at X-band frequencies (~9.4 GHz) using a MiniScope MS-5000 benchtop EPR spectrometer (Freiberg Instruments, Germany). Magnetic field modulation and lock-in detection were used, leading to a derivative spectrum. The Q factor of the empty rectangular resonator (TE 102 with constant B_1 distribution in a +/− 6 mm range in the direction of the cylindrical sample) is 2520. The measurements were performed at a microwave power of 5.01 mW with a modulation frequency of 100 kHz and a modulation amplitude of 0.3 mT, using 60 s and 20 s sweep time per cycle for *ex situ* and *in situ* measurements respectively. The number of spins was determined from the double integral of the experimental spectrum, taking into account the experimental settings and the Q factor of the resonator,

automatically recorded by the spectrometer software ESRStudio 1.72.1 prior to each scan. A linear baseline was subtracted from the spectra before double integration.

For better data representation, several spectra were smoothed using Easyspin's [28] 'datasmooth' function. A reference sample (4-hydroxy-TEMPO, also known as TEMPOL, dissolved in toluene) with a known number of spins was measured to obtain the reference integrated EPR signal amplitude, for comparison to the systems of interest where we intend to determine the number of spins. The uncertainty in the absolute number of spins is less than 20 %.

3. Results and discussion

3.1. Electrochemical sample deposition and cleaning

For preparing the sample for *in situ* experiments, the WE as well as the external CE and RE were immersed in a beaker (vial ROTILABO 4 ml, Ø 1.5 cm) with a solution containing 1 mM monomer in 0.1 M Et_4NBF_4 / CH_3CN. The polymer films were prepared by electrochemical polymerisation as previously reported for a similar material (DiTS) containing a succinyl TEMPO bearing linker [14,29]. Polymerisation was conducted in the potential range from −0.4 V to +0.9 V with a potential sweep rate of 50 mV s^{-1} for 10 cycles. The CV curves show oxidation of the monomer between 0.6 V and 0.9 V and oxidation / reduction of TEMPO around 0.4 V. An increase in current in this region is noticeable from cycle to cycle, indicating increasing thickness of the deposited layer (Fig. 3a).

After deposition, the polymer film was subjected to a cleaning procedure to remove monomer particles from pores in the polymer film. The unchanged cell was immersed in acetonitrile solution for 2 min. Subsequently, several CVs were recorded in an electrolyte in a beaker that did not contain any monomers. This cycle was repeated 3 times. Afterwards, the film was dried in air for 5 min to ensure that remaining acetonitrile was evaporated from the sample. After this, the polymer was tested in a fresh electrolyte solution in a beaker. In contrast to the DiTS material studied previously [29], the electrochemical activity region of deposited polymer metal-organic backbone shifts towards negative potentials from 0.4 V for pDiTS to 0–0.2 V for pDiTBuS (Fig. 3b). This effect is due to the succinyl fragment being electron-withdrawing both by inductive and by mesomeric mechanisms increasing the energy required for the ligand oxidation. In contrast, the ether linker of DiTBuS has an electron-donating mesomeric effect, so that depletion of the electron density in the benzene ring does not occur, which facilitates oxidation.

3.2. Influence of sample position on EPR performance

First, the cell was inserted into the shell without electrolyte, and cwEPR measurements were carried out in the centre of the resonator as well as at a distance of 5 mm above the resonator centre (Fig. S2a). The distance discussed here is the distance between the centre of the resonator and the centre of the WE's spiral part. Inserting a cell without electrolyte at a distance of 5 mm from the centre of the resonator reduces the *Q* factor to 2160. Inserting the cell into the centre of the resonator further reduces *Q* to 1860. In the reduced state of the polymer, only the TEMPO groups are EPR active, and the spectrum of the discharged film exhibits a single Lorentzian derivative line (with peak-to-peak linewidth $Lw_{pp} \sim 1.25$ mT, g ~ 2.0062). The single line observed here, similar as for pDiTS [14], is due to strong dipolar and exchange coupling between the TEMPO radicals within the densely packed film. The number of unpaired electrons in the film located in the centre of the resonator was determined by double integration of the spectra to be 1.15×10^{16} (with up to ±20 % error in quantitative cwEPR). This is about 10 % less than the number of electrochemically active TEMPO charges (1.28×10^{16}) as determined by integration of the cathodic wave of the CV of the cell *vs.* time. This discrepancy can be attributed to partial antiferromagnetic coupling between nearby spins forming diamagnetic (EPR silent) states [30], as well as a slight interaction of the sample with the electric field of the resonator, which leads to an asymmetry of the spectrum and affects the accuracy of the quantitative EPR analysis. A measurement was also carried out on the same sample pulled up to a distance of 5 mm from the centre of the resonator (*cf.* Fig. S2a). The double-integrated signal intensity determined by the quantitative EPR analysis at this sample position was reduced by about 60 %.

For the sample immersed in electrolyte, a similar result was obtained, with an admixture of the dispersion signal caused by the strong interaction between the polar electrolyte and the microwave electric field in the resonator, resulting in a more asymmetric spectrum (Fig. S2b, Fig. 4). To fit the obtained signals, the 'microwave phase' parameter in the EasySpin tool box was used as a fit parameter to adjust the absorption/dispersion admixture. A series of measurements was performed in which the position of the sample was varied relative to the centre of the resonator. This allowed us to assess the influence of the sample position on the *Q* factor, number of spins obtained by quantitative EPR as well as the asymmetry of the spectrum.

Fig. 4 shows monotonic dependencies of these parameters on the distance of the sample to the resonator centre. The symmetry of the signal weakly depends on the distance, and only for distances larger than

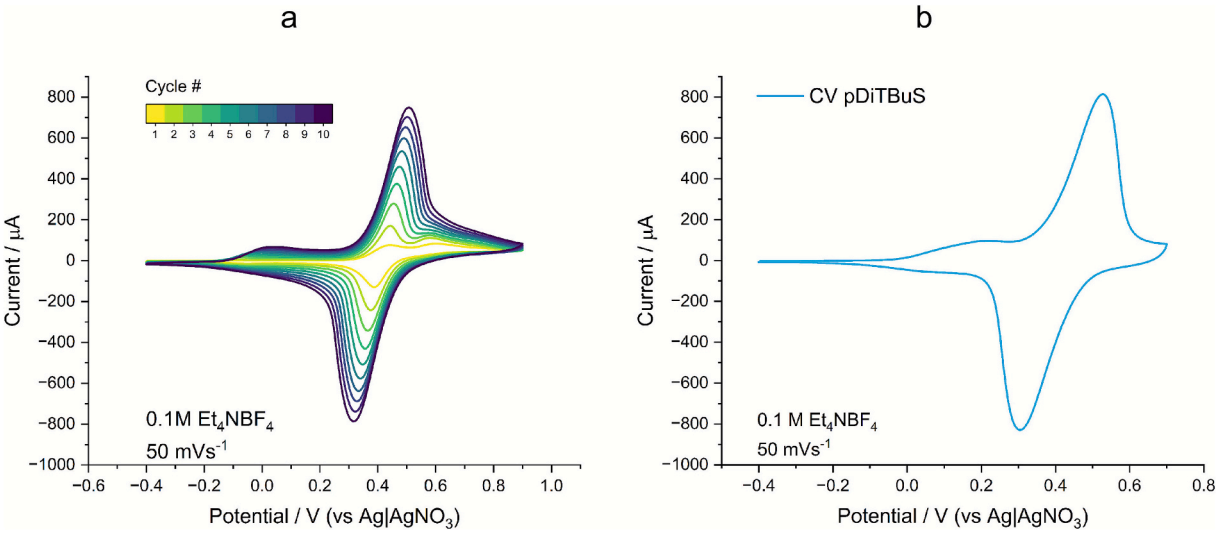


Fig. 3. Electrodeposition of DiTBuS from 1 mM monomer electrolyte solution in CV mode (a); CV of a pDiTBuS film in pure electrolyte solution (b) using a scan rate of 50 mV s^{-1} in both cases.

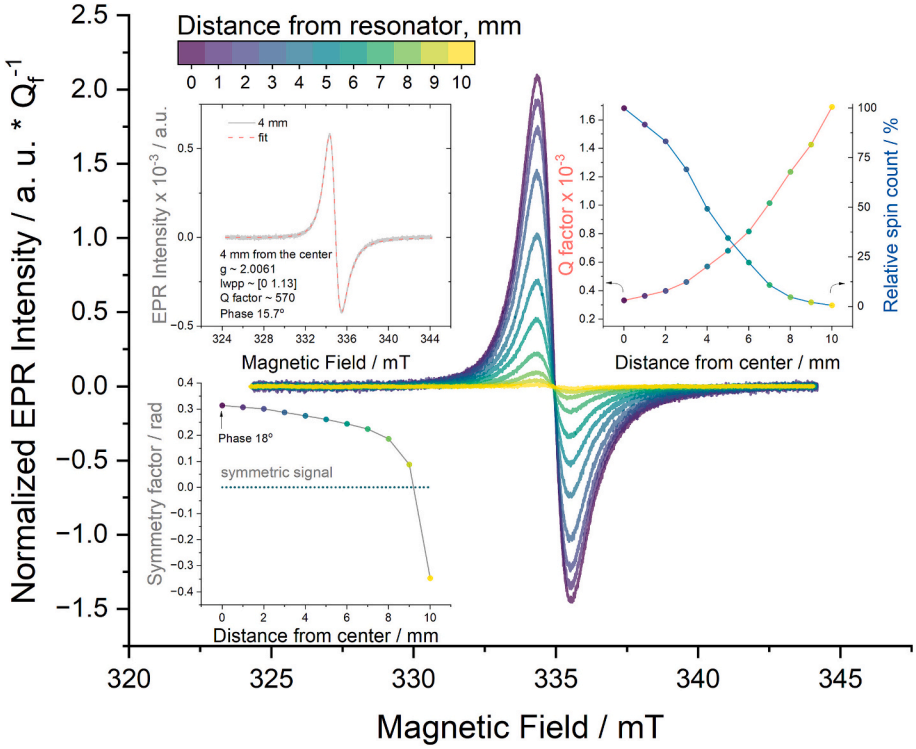


Fig. 4. cwEPR spectra of a pDiTBuS polymer film in 1 M Et_4NBF_4 / CH_3CN with the sample positioned at different distances from the resonator centre. The insets show the dependence of the *Q* factor, spin count and asymmetry factor (representation of absorption and dispersion behaviour, using the microwave phase in rad as a fit parameter) on the distance of the sample from the resonator centre.

9 mm significant changes in the spectrum caused by low signal to noise ratio can be observed (Fig. S2c). *Q* factor and number of spins show inverse dependencies. Prolonged measurements in the region of minimum tolerable *Q* factors (*i.e.* in our case in close distance to the resonator centre) often lead to the loss of critical coupling. For this reason, all subsequent measurements presented here were performed at a distance of 4 mm from the resonator centre.

3.3. *In situ film-electrochemical EPR measurements*

To assess the capabilities of the electrochemical cell, a number of different tests were carried out: (1) simultaneous CV in combination with cwEPR, (2) CV in combination with static measurements of the cwEPR signal intensity at fixed magnetic field, as well as (3) *in situ* GCD measurements. Fig. 5a shows the CV of pDiTBuS obtained at a potential scan rate of 5 mV s^{-1}. The CV shows activity of the conductive backbone in the 0.4–0.6 V region, as well as a TEMPO/$TEMPO^+$ pair of peaks at 0.77 V with a peak separation of 62 mV. In this configuration, it was possible to achieve a significant improvement in the electrochemical response compared to the results obtained for pDiTS under the same test conditions in a flat cell configuration [14]. During the CV sweeps, the cwEPR spectra were recorded every 140 mV (corresponding to 28 s), at a microwave power of 5.01 mW (non-saturating conditions) and a modulation amplitude of 0.3 mT (Fig. 5b). Up to ~0.6 V, the spectrum exhibits one broad line that is attributed to TEMPO groups in the solid phase. In the region between 0.6 V and 0.7 V, oxidation of TEMPO groups sets in, leading to a dilution of the local spin density, signal broadening and a decrease in intensity (Fig. S3). Upon further oxidation of the film, a transition to a three-line spectrum is observed, caused by hyperfine interaction of individual TEMPO groups, followed by complete disappearance of the signal when the film is fully oxidized. Upon reduction, the opposite picture is observed, associated with a return to the single-line spectrum. The efficiency of the aforementioned oxidation process can be estimated using the double integral (DI) of the obtained EPR signal and was found to be approximately 98 %, leaving about 2 % of TEMPO groups in their paramagnetic state (Fig. 5a). This fact excludes the possible shielding effect of closely spaced TEMPO groups, in which the oxidation of one group blocks the oxidation of the other [31]. As in the case of pDiTS [14], polaron signals, which usually exhibit a broad signal with a *g* factor different from the *g* factor of the TEMPO radical (~2.008/2.011) [32], were not detected. The reason for the absence of a clear NiSalen signal is possibly related to the formation of diamagnetic species due to partial antiferromagnetic coupling between nearby TEMPO radical and polaron spins [30], which was previously also observed for Cu based Salen type backbones [33].

One of the key features of the cell presented here is the possibility of operating at relatively high potential sweep rates while maintaining a stable electrochemical response. As an example, Fig. 5c and Fig. S4 show the results of *in situ* experiments recorded with a sweep rate of 10–30 mV s^{-1}. Since it is impossible to simultaneously record cwEPR spectra without losing data quality due to averaging over a significant range of potentials, an analysis of the signal intensity obtained at a fixed magnetic field was performed. The single-field-point (SFP) measurement was carried out at 335.5 mT, which corresponds to the minimum of the first derivative obtained during the cwEPR test experiments (marked with arrows in Fig. 5b). The intensity at this point is taken with positive sign, and a decrease in the signal intensity during oxidation until zero and an increase during reduction are observed. It should be noted that in the SFP mode, the onset of the oxidation process begins at 0.4 V, *i.e.* 200 mV lower than previously determined by double integration of the cwEPR spectra (Fig. 5a). This effect occurs due to line broadening during oxidation, which significantly reduces the signal intensity at fixed magnetic field while maintaining the double integral values (Fig. S3). When representing the intensity minima of standard cwEPR spectra in the same manner (values with a positive sign, coloured dots in Fig. 5c), the dependencies almost completely coincide. This means that the SFP signal provides more reliable information on the onset of any processes occurring during oxidation and reduction that involve changes in local

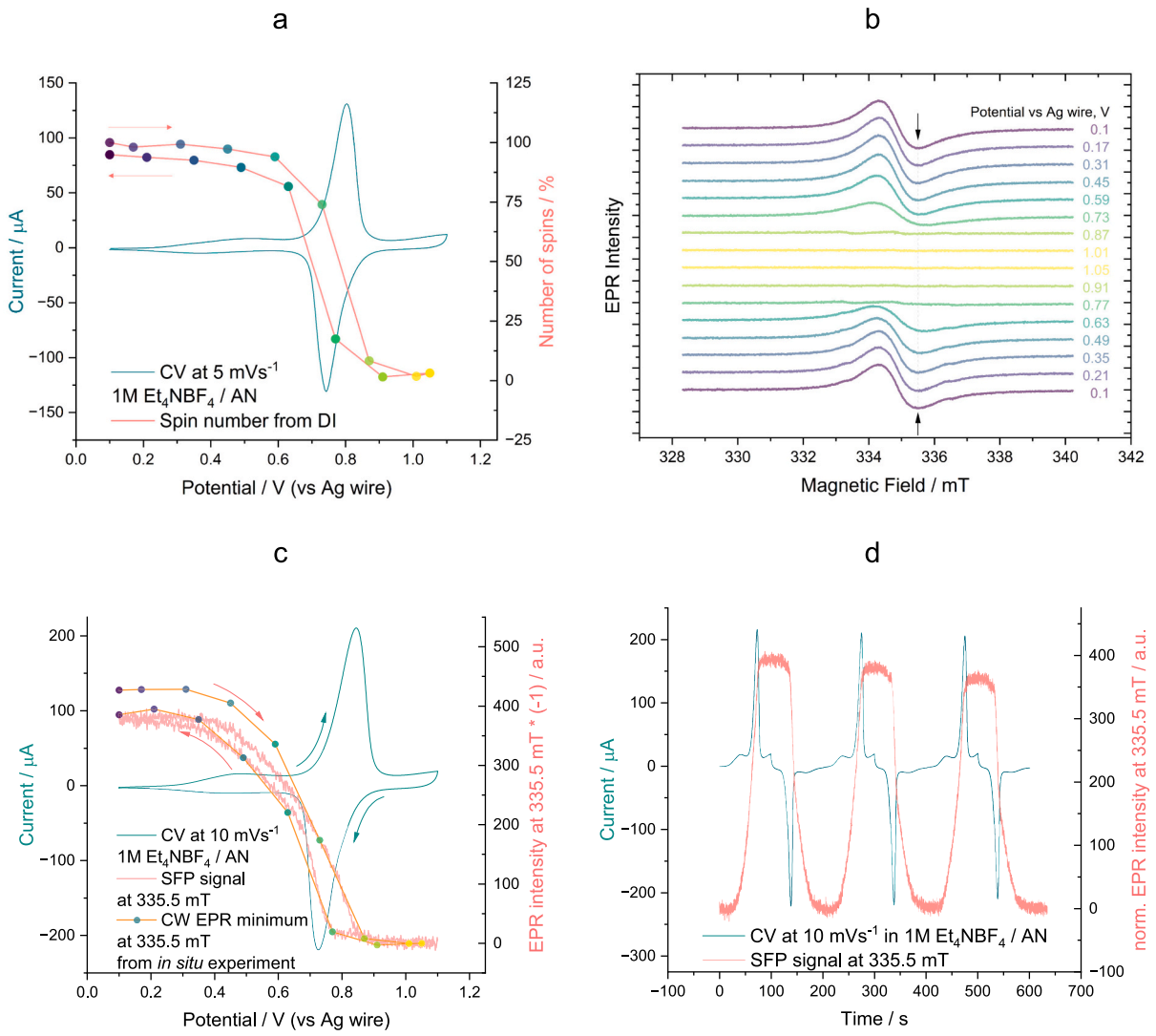


Fig. 5. CV and number of spins for the *in situ* measurements recorded at 5 mV s^{-1} (a) and corresponding cwEPR spectra recorded every 140 mV (b); CV, signal intensity of *in situ* and single-field-point signal recorded at 10 mVs^{-1} (c) and single-field-point signal intensity *vs.* time detected during three full CV cycles (d); all experiments were carried out in 1 M Et_4NBF_4 / CH_3CN electrolyte solution.

spin density. In contrast, double integration of the cwEPR spectra gives the state of charge at a particular potential.

In the region between 0.4 V and 0.6 V, only the polymer backbone activity is observed in the CV, which in theory should only lead to an increase in the cwEPR signal intensity due to the generation of additional cation radicals or polarons. A decrease in intensity and signal broadening can be a consequence of the antiferromagnetic interaction of densely packed TEMPO groups with polarons formed during oxidation. Considering a low polymer doping level at the onset of oxidation, the ratio between the concentrations of polarons and TEMPO radicals should be low. The presence of polarons, which remain in the paramagnetic state, can be masked by the broad TEMPO signal.

A decrease in the electrochemical and EPR signal intensities was observed when the sweep rate is increased (Fig. S5). This effect can be attributed to kinetic or diffusion limitation of the oxidation process for high sweep rates, which leads to a significant decrease in the current [34]. Depending on the sweep rate (Fig. S4), a small shift in the potential range of the polymer backbone activity, as well as of the onset of the cwEPR intensity changes can be observed. At the same time, the shape of the SFP signal dependence appears scan-rate independent, although the onset of the SFP intensity change remains linked to the appearance of the electrochemical activity of the polymer backbone. This confirms the influence of the activity of the metal-organic backbone on the EPR pattern.

Since a decrease in signal intensity is observed over three cycles (Fig. 5d, Fig. S5) as well as a drop in current after all previous tests, we assume that degradation of the material occurs during the measurements. To analyse the degradation process and to test the capabilities of the developed cell, an analysis of strong oxidative overcharge was carried out using the GCD method. In this technique, a constant current is applied to charge and discharge a material, and the resulting voltage is recorded over time. It provides insights into the material's capacity, coulombic efficiency, and stability during repeated cycling. For the degradation analysis, a constant current was applied to the cell until a potential beyond the stability range was reached, and the EPR spectrum was simultaneously recorded every 20 s, followed by a reduction to the initial state. Fig. 6a and Fig. S6a provide an overview of the changes that the sample underwent during overcharging. A consistent decrease in intensity of the broad line in the reduced polymer state is seen, along with the appearance and increase in intensity of the three-line spectrum in the oxidized polymer state. The three-line spectrum is preserved even in the reduced polymer state. Fig. S6b also shows a gradual decrease in the material capacity during GCD.

Fig. 6b shows the spectral distortion after five cycles of oxidative

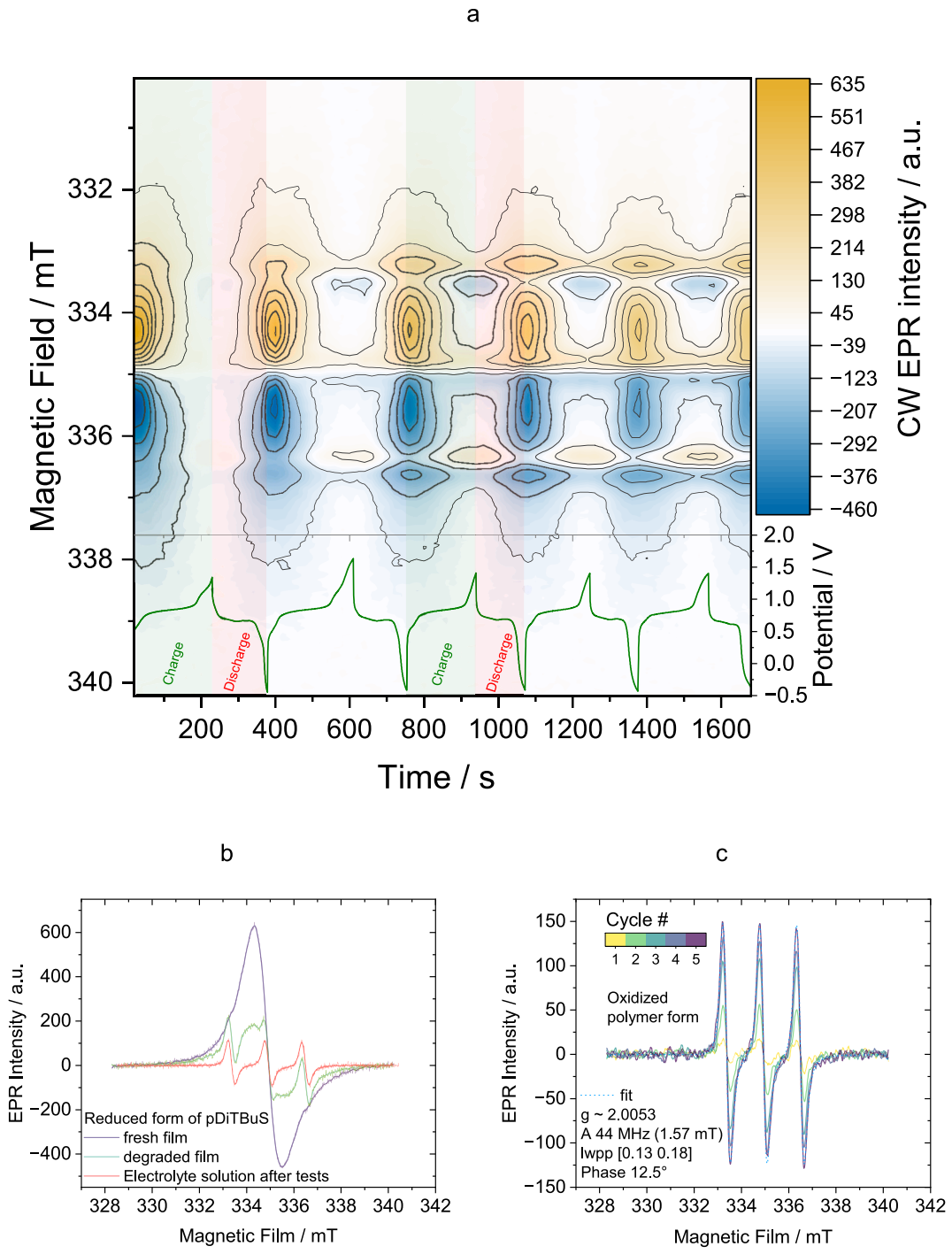


Fig. 6. Results of *in situ* cwEPR experiments coupled with a GCD overcharging process (a) recorded at 25C (0.126 mA cm^{-2} or 18 μA); comparison of the signal of the reduced (b) and oxidized (c) forms of the polymer during the experiment along with the spectrum of the electrolyte.

overcharge, a decrease in the intensity of the broad band and the appearance of the three-line spectrum. An analysis of the used electrolyte after removing the sample from the shell also reveals a three-line spectrum of nitroxyl groups, which coincides with the spectrum of the polymer in the oxidized form (Fig. 6c). This figure shows that degradation sets in immediately after the first cycle and continues gradually from cycle to cycle for the same film, leading to an increase in the intensity of the three-line spectrum. Considering that a five-line spectrum is expected from the monomeric fragment, caused by exchange coupling between two neighbouring TEMPO groups [14,35,36], we conclude that degradation is most likely linked to the cleavage of a linker fragment.

4. Conclusion

A simple and cost-effective design of an *in situ* electrochemical cell for room-temperature cwEPR measurements of redox-active polymer films in polar electrolytes was presented. Its operational parameters and capabilities were analysed in detail using a TEMPO-containing RCP material as an example. The possibility of obtaining reliable electrochemical signals was demonstrated for various sweep rates. It was shown that recording full cwEPR spectra gives the most reliable results for determining the material's state of charge. In contrast, conducting experiments at a fixed magnetic-field position allows accurate

determination of the onset of oxidation and reduction processes.

The cell can be used to investigate basic electrochemical parameters and degradation processes at room temperature. Further, the stability and activity windows of the individual components of the systems under study can be explored. The cell is suitable for *in situ* experiments in potentiostatic, galvanostatic and potentiodynamic modes. Since the cell is compatible with commercially available benchtop EPR spectrometers, temperature-dependent measurements (above the freezing point of the electrolyte) are easily accessible. Being reusable and inexpensive, the cell demonstrates high flexibility for possible modifications while maintaining a balance between the quality of electrochemical and EPR data. Depending on the system under study, it should be possible to modify the setup easily using 3D printing, various polymer materials and glass for the shell composition. The main criteria for the successful operation of the cell are the conical shape of the shell (which reduces the electrolyte volume), electrode insulation and positioning of the electrodes relative to each other. Gold, platinum, palladium, silver WEs of various diameters and shapes can be used, tailored to the characteristics of the resonator and signal intensity of the sample deposited onto the working electrode. The latter can be significantly boosted by changing the working surface area of the electrodes. This setup is suitable to study a wide variety of redox-active materials, not limited to RCPs.

CRediT authorship contribution statement

Anatoliy A. Vereshchagin: Writing – review & editing, Writing – original draft, Visualization, Resources, Methodology, Investigation, Formal analysis, Conceptualization. **Maryam Seif-Eddine:** Writing – review & editing, Visualization. **Kaltum Abdiaziz:** Writing – review & editing, Methodology. **Maxie M. Roessler:** Writing – review & editing, Conceptualization. **Oleg V. Levin:** Resources, Funding acquisition. **Jan Behrends:** Writing – review & editing, Supervision, Funding acquisition, Conceptualization.

Funding

This work was supported by the joint Russian Science Foundation (RSF)-DFG grant program (RSF grant number 22–43-04414, DFG grant number BE 5126/7–1).

Declaration of competing interest

The authors declare that they have no known competing financial interests or personal relationships that could have appeared to influence the work reported in this paper.

Acknowledgments

The design of the new molecule under study and its synthesis were carried out at Saint Petersburg State University in the Department of Electrochemistry.

Appendix A. Supplementary data

Supplementary data to this article can be found online at https://doi.org/10.1016/j.jmr.2025.108010.

Data availability

Data will be made available on request.

References

[1] K. Abdiaziz, E. Salvadori, K.P. Sokol, E. Reisner, M.M. Roessler, Protein film electrochemical EPR spectroscopy as a technique to investigate redox reactions in biomolecules, Chem. Commun. 55 (2019) 8840–8843, https://doi.org/10.1039/C9CC03212F.

[2] D. Facchetti, Y. Dang, M. Seif-Eddine, B.L. Geoghegan, M.M. Roessler, Film-electrochemical EPR spectroscopy to investigate electron transfer in membrane proteins in their native environment, Chem. Commun. 60 (2024) 12690–12693, https://doi.org/10.1039/D4CC04013A.

[3] B. Kastening, B. Gostiša-Mihelčić, J. Divišek, E.S.R. Investigations of short-lived intermediates in electrochemical reactions, faraday discuss, Chem. Soc. 56 (1973) 341–352, https://doi.org/10.1039/DC9735600341.

[4] B. Kastening, Anwendung der Elektronenspinresonanz in der organischen Elektrochemie, Chemie Ing. Tech. 42 (1970) 190–195, https://doi.org/10.1002/cite.330420409.

[5] Y. Kutin, N. Cox, W. Lubitz, A. Schnegg, O. Rüdiger, In situ EPR characterization of a cobalt oxide water oxidation catalyst at neutral pH, Catalysts 9 (2019) 926, https://doi.org/10.3390/catal9110926.

[6] S.A. Bonke, T. Risse, A. Schnegg, A. Brückner, In situ electron paramagnetic resonance spectroscopy for catalysis, Nat. Rev. Methods Primers 1 (2021) 33, https://doi.org/10.1038/s43586-021-00031-4.

[7] S. Neukermans, M. Samanipour, H.Y. Vincent Ching, J. Hereijgers, S. Van Doorslaer, A. Hubin, T. Breugelmans, A versatile in-situ electron paramagnetic resonance spectro-electrochemical approach for electrocatalyst research, ChemElectroChem 7 (2020) 4578–4586, https://doi.org/10.1002/celc.202001193.

[8] J.B. Priebe, M. Karnahl, H. Junge, M. Beller, D. Hollmann, A. Brückner, Water reduction with visible light: synergy between optical transitions and electron transfer in Au-TiO 2 catalysts visualized by in situ EPR spectroscopy, Angew. Chem. Int. Ed. 52 (2013) 11420–11424, https://doi.org/10.1002/anie.201306504.

[9] M. Seif-Eddine, S.J. Cobb, Y. Dang, K. Abdiaziz, M.A. Bajada, E. Reisner, M. M. Roessler, Operando film-electrochemical EPR spectroscopy tracks radical intermediates in surface-immobilized catalysts, Nat. Chem. 16 (2024) 1015–1023, https://doi.org/10.1038/s41557-024-01450-y.

[10] M. Sathiya, J.-B. Leriche, E. Salager, D. Gourier, J.-M. Tarascon, H. Vezin, Electron paramagnetic resonance imaging for real-time monitoring of li-ion batteries, Nat. Commun. 6 (2015) 6276, https://doi.org/10.1038/ncomms7276.

[11] J. Wandt, C. Marino, H.A. Gasteiger, P. Jakes, R.-A. Eichel, J. Granwehr, Operando electron paramagnetic resonance spectroscopy – formation of mossy lithium on lithium anodes during charge–discharge cycling, Energy Environ. Sci. 8 (2015) 1358–1367, https://doi.org/10.1039/C4EE02730B.

[12] A. Niemöller, P. Jakes, S. Eurich, A. Paulus, H. Kungl, R.-A. Eichel, J. Granwehr, Monitoring local redox processes in LiNi0.5Mn1.5O4 battery cathode material by in operando EPR spectroscopy, J. Chem. Phys. 148 (2018), https://doi.org/10.1063/1.5008251.

[13] E.W. Zhao, E. Jónsson, R.B. Jethwa, D. Hey, D. Lyu, A. Brookfield, P.A.A. Klusener, D. Collison, C.P. Grey, Coupled in situ NMR and EPR studies reveal the electron transfer rate and electrolyte decomposition in redox flow batteries, J. Am. Chem. Soc. 143 (2021) 1885–1895, https://doi.org/10.1021/jacs.0c10650.

[14] I. Kulikov, N.A. Panjwani, A.A. Vereshchagin, D. Spallek, D.A. Lukianov, E. V. Alekseeva, O.V. Levin, J. Behrends, Spins at work: probing charging and discharging of organic radical batteries by electron paramagnetic resonance spectroscopy, Energy Environ. Sci. 15 (2022) 3275–3290, https://doi.org/10.1039/D2EE01149B.

[15] S. den Hartog, S. Neukermans, M. Samanipour, H.Y.V. Ching, T. Breugelmans, A. Hubin, J. Ustarroz, Electrocatalysis under a magnetic lens: a combined electrochemistry and electron paramagnetic resonance review, Electrochim. Acta 407 (2022) 139704, https://doi.org/10.1016/j.electacta.2021.139704.

[16] R.N. Bagchi, A.M. Bond, F. Scholz, ESR-electrochemical cells and their performance in studies of redox processes, Electroanalysis 1 (1989) 1–11, https://doi.org/10.1002/elan.1140010103.

[17] D.K.F. Bruyers, S. Richert, Design of an electrochemical cell for continuous wave EPR measurements of radical ions, Chemistry 30 (2024) e202402719, https://doi.org/10.1002/chem.202402719.

[18] I.B. Goldberg, A.J. Bard, S.W. Feldberg, Resistive effects in thin electrochemical cells. Digital simulations of electrochemistry in electron spin resonance cells, J. Phys. Chem. 76 (1972) 2550–2559, https://doi.org/10.1021/j100662a013.

[19] R.N. Bagchi, A.M. Bond, R. Colton, Simultaneous in-situ electron spin resonance and voltammetric studies in high resistance solvents at low temperatures using a newly designed small volume electrolysis cell, J. Electroanal. Chem. Interfacial Electrochem. 199 (1986) 297–309, https://doi.org/10.1016/0022-0728(86)80005-5.

[20] M.A. Tamski, J.V. Macpherson, P.R. Unwin, M.E. Newton, Electrochemical electron paramagnetic resonance utilizing loop gap resonators and micro-electrochemical cells, Phys. Chem. Chem. Phys. 17 (2015) 23438–23447, https://doi.org/10.1039/C5CP04259C.

[21] A.A. Vereshchagin, A.Y. Kalnin, A.I. Volkov, D.A. Lukyanov, O.V. Levin, Key features of TEMPO-containing polymers for energy storage and catalytic systems, Energies 15 (2022) 2699, https://doi.org/10.3390/en15072699.

[22] E.-T. Liu, S.-L. Mei, X.-H. Chen, C.-J. Yao, Conducting polymers with redox active pendant groups: their application progress as organic electrode materials for rechargeable batteries, J. Mater. Chem. C 10 (2022) 13570–13589, https://doi.org/10.1039/D2TC01150F.

[23] J. Chen, C.O. Too, G.G. Wallace, G.F. Swiegers, B.W. Skelton, A.H. White, Redox-active conducting polymers incorporating ferrocenes. Preparation, characterization and bio-sensing properties of ferrocenylpropyl and -butyl polypyrroles, Electrochim. Acta 47 (2002) 4227–4238, https://doi.org/10.1016/S0013-4686(02)00446-2.

[24] P.H. Rieger, I. Bernal, W.H. Reinmuth, G.K. Fraenkel, Electron spin resonance of electrolytically generated nitrile radicals, J. Am. Chem. Soc. 85 (1963) 683–693, https://doi.org/10.1021/ja00889a010.

[25] P.R. Murray, D. Collison, S. Daff, N. Austin, R. Edge, B.W. Flynn, L. Jack, F. Leroux, E.J.L. McInnes, A.F. Murray, D. Sells, T. Stevenson, J. Wolowska, L.J. Yellowlees, An in situ electrochemical cell for Q- and W-band EPR spectroscopy, J. Magn. Reson. 213 (2011) 206–209, https://doi.org/10.1016/j.jmr.2011.09.041.
[26] A.A. Vereshchagin, J.V. Novoselova, A.Y. Kalnin, D.A. Lukyanov, 2-Hydroxy-3-(4-oxy(2,2,6,6-tetramethylpiperidin-1-oxyl)butoxy)benzaldehyde, Molbank 2021 (2021) M1245, https://doi.org/10.3390/M1245.
[27] V.V. Pavlishchuk, A.W. Addison, Conversion constants for redox potentials measured versus different reference electrodes in acetonitrile solutions at 25°C, Inorg. Chim. Acta 298 (2000) 97–102, https://doi.org/10.1016/S0020-1693(99)00407-7.
[28] S. Stoll, A. Schweiger, EasySpin, a comprehensive software package for spectral simulation and analysis in EPR, J. Magn. Reson. 178 (2006) 42–55, https://doi.org/10.1016/j.jmr.2005.08.013.
[29] A.A. Vereshchagin, D.A. Lukyanov, I.R. Kulikov, N.A. Panjwani, E.A. Alekseeva, J. Behrends, O.V. Levin, The fast and the capacious: a [Ni(Salen)]-TEMPO redox-conducting polymer for organic batteries, Batteries Supercaps 4 (2021) 336–346, https://doi.org/10.1002/batt.202000220.
[30] A. Privitera, R. Warren, G. Londi, P. Kaienburg, J. Liu, A. Sperlich, A.E. Lauritzen, O. Thimm, A. Ardavan, D. Beljonne, M. Riede, Electron spin as fingerprint for charge generation and transport in doped organic semiconductors, J. Mater. Chem. C 9 (2021) 2944–2954, https://doi.org/10.1039/D0TC06097F.
[31] T. Katsumata, M. Satoh, J. Wada, M. Shiotsuki, F. Sanda, T. Masuda, Polyacetylene and polynorbornene derivatives carrying TEMPO. Synthesis and properties as organic radical battery materials, Macromol. Rapid Commun. 27 (2006) 1206–1211, https://doi.org/10.1002/marc.200600286.
[32] E. Dmitrieva, M. Rosenkranz, J.S. Danilova, E.A. Smirnova, M.P. Karushev, I. A. Chepurnaya, A.M. Timonov, Radical formation in polymeric nickel complexes with N2O2 Schiff base ligands: an in situ ESR and UV–vis–NIR spectroelectrochemical study, Electrochim. Acta 283 (2018) 1742–1752, https://doi.org/10.1016/j.electacta.2018.07.131.
[33] J.S. Danilova, E. Dmitrieva, A.M. Timonov, ESR, UV–vis–NIR and FTIR spectroscopic characterization of charge carriers in copper salen polymeric complexes, J. Electroanal. Chem. 970 (2024) 118549, https://doi.org/10.1016/j.jelechem.2024.118549.
[34] H. Lindström, S. Södergren, A. Solbrand, H. Rensmo, J. Hjelm, A. Hagfeldt, S.-E. Lindquist, Li + ion insertion in TiO 2 (anatase). 2. voltammetry on nanoporous films, J. Phys. Chem. B 101 (1997) 7717–7722, https://doi.org/10.1021/jp970490q.
[35] A.A. Vereshchagin, U.M. Rodionova, A.G. Dolmatova, S.S. Suglobov, J. Behrends, E.V. Alekseeva, 6,6′-{[Ethane-1,2-diylbis(azaneylylidene)]bis(methaneylylidene)}bis[(1-oxyl-2,2,5,5-tetramethylpyrrolidine-3-carboxy)phenolato] nickel(II), Molbank 2025 (2025) M1964, https://doi.org/10.3390/M1964.
[36] A.A. Vereshchagin, U.M. Rodionova, A.G. Dolmatova, S.D. Suglobov, J. Behrends, E.V. Alekseeva, 6,6′-{[Ethane-1,2-Diylbis(azaneylylidene)]bis(methaneylylidene)}bis[2-(4-oxy(2,2,6,6-Tetramethylpiperidin-1-Oxyl)butyloxy)phenolato] cobalt(II), Molbank 2025 (2025) M1959, https://doi.org/10.3390/M1959.